Journal of Thermal Analysis and Calorimetry (2020) 139:2623–2631
https://doi.org/10.1007/s10973-019-08684-w

Investigation of energy performance in a U-shaped evacuated solar tube collector using oxide added nanoparticles through the emitter, absorber and transmittal environments via discrete ordinates radiation method

Yeping Peng[1] · Ali Zahedidastjerdi[2] · Ali Abdollahi[2] · Atefeh Amindoust[3] · Mehrdad Bahrami[2] · Arash Karimipour[2] · Marjan Goodarzi[4]

Received: 29 June 2019 / Accepted: 9 August 2019 / Published online: 26 August 2019

Abstract
This work is a three-dimensional numerical study of a U-shaped evacuated tube solar collector employing different types of oxide nanofluids including water–Al_2O_3, water–CuO and water–TiO_2 under the steady-state condition. The simulation is performed using the single-phase method for nanofluid modeling, the DO method for radiation modeling, incompressible and fluid flow laminar regime. The thermo-physical properties of the water are considered as a function of temperature ranging from 0 to 150 °C. The obtained results showed that increasing both length and diameter of the U-shaped tubes of the solar collector enhances its thermal efficiency. Moreover, it is found that using oxide nanofluids results in an enhancement in the collector thermal performance which using water–CuO nanofluid causes 13.8, 1.5 and 1.3% higher collector thermal efficiency in comparison with employing pure water, water–TiO_2 and water–Al_2O_3 nanofluids, respectively. It is also observed that the working fluid heat capacity plays an important role in the thermal performance of the evacuated tube solar collector.

Keywords Energy performance · Solar collector · Oxide nanofluid · U-shaped tube

Introduction

The economic growth of human societies involves the energy issue, one of the least costly and most commonly used energies, solar energy, which has led many researchers to this end. Nature and mankind have devised various ways to use solar energy. In fact, the easiest use is to convert energy from solar radiation to thermal energy. Hence, various solar water heater systems have been built and used. One of the ways to convert the solar energy to thermal energy is to use U-shaped tube collectors.

Among the evacuated tube solar collectors, the most common type is the all-glass evacuated tubes to transfer the solar energy directly to the fluid circulating in it. Morrison et al. [1] investigated the performance of a water-in-glass evacuated tube solar preheater using the International Standard test method ISO 9459-2 for a range of locations in Asia and Europe. They showed that an inactive region near the sealed end of the tube exists based on their numerical simulation of water circulation through long single-ended thermosyphon tubes. Morrison et al. [2] in another study evaluated the characteristics of water-in-glass evacuated tube solar water heaters including assessment of the circulation rate through single-ended tubes

✉ Marjan Goodarzi
marjan.goodarzi@tdtu.edu.vn

[1] Shenzhen Key Laboratory of Electromagnetic Control, College of Mechatronics and Control Engineering, Shenzhen University, Shenzhen 518060, China

[2] Department of Mechanical Engineering, Najafabad Branch, Islamic Azad University, Najafabad, Iran

[3] Department of Industrial Engineering, Najafabad Branch, Islamic Azad University, Najafabad, Iran

[4] Sustainable Management of Natural Resources and Environment Research Group, Faculty of Environment and Labour Safety, Ton Duc Thang University, Ho Chi Minh City, Vietnam

numerically and experimentally. To validate their numerical work, they used particle image velocimetry (PIV) for flow measurement. These researchers developed a non-dimensional correlation of the circulation rate through a single evacuated tube mounted at 45° inclination over a diffuse reflector. Later, Budihardjo et al. [3] performed a numerical and experimental study to develop the correlation proposed by Morrison et al. [2]. They also investigated the sensitivity of the flow rate correlation to the variation in circumferential heat flux distribution. Benedetto et al. [4] analyzed the water-in-glass evacuated tube solar collectors using commercial software of Fluent based on CFD numerically. They simulated a horizontal tube and just one part of the entire collector for simplicity. They performed their simulations for pipe length between 0.59 and 1.1.47 m, mass flow rate between 0.05 and 10 kg min^{-1} and inlet temperature of 333 K. They found that collectors with lower pipe length have higher efficiencies, the optimum mass flow rate for the inlet flow is between 0.4 and 1 kg min^{-1}, and the fluid flow structure in the collector does not change much with the fluid mass flow rate. Ong and Chow [5] performed a comparison on evacuated tube collectors (U-shaped tube and heat-pipe design). They reported that the evacuated tube collector with heat-pipe design has a higher efficiency and lower-temperature drop during the night [6]. Rittidech et al. [7] investigated the thermal performance of a closed-end oscillating heat pipe experimentally. They employed R123, ethanol and water as the working fluids with a filling ratio of 50%. Their experiment results showed that the correlation equation could predict the heat flux and that the operation map could predict the operational range and the inner diameter. Hayek et al. [8] studied an experimental investigation of solar collectors under local weather conditions as encountered along the eastern coast of the Mediterranean Sea which is carried out for two kinds of evacuated tube solar collectors, namely the water-in-glass tubes and the heat-pipe designs. Their results showed that although the heat-pipe-based collectors have higher efficiency, almost 15–20%, than the water-in-glass designs, their payback periods are much higher due to their larger production cost. Sawhney et al. [9] provided a model for the thermal efficiency of a U-shaped evacuated tube solar collector connected to a flat absorber. They examined the distribution of fluid temperature along the U-shaped tube. Investigated the efficiency of the evacuated tube collector with four different absorber shapes numerically was also reported [10]. These four shapes were: blade tubes, U-shaped tubes welded into an annulus blade, a U-shaped tube welded into a copper absorber plate and a U-shaped tube welded into a rectangular duct. Their results showed that the U-shaped tube welded into the annulus blade has the best efficiency among the four absorber shapes, while taking into account the effects of adjacent tubes, the U-shaped tube welded into the copper absorber plate has the best efficiency at all radiation angles. Diaz [11] analyzed the performance of an evacuated tube solar collector that contains a U-shaped mini-channel tube. His results showed that this type of collectors has 5% higher thermal performance than the standard U-shaped round-tube solar collectors. Moreover, the design of a mini-channel-based solar collector without absorber fin is evaluated and its performance optimized due to its geometrical parameters. Liang et al. [12] proposed the filled-type evacuated solar collector with single U-tube using compressed graphite benefiting from its high thermal conductivity to omit the effect of thermal resistance between the absorber tube and the copper fin of the conventional U-shaped evacuated tube solar collectors. Later, Liang et al. [13] developed their previous work and investigated the filled-type evacuated solar collector with double U-tube. They compared the single and double U-tube in at the same working conditions. Yousefi et al. [14] performed an experimental study of the effect of Al_2O_3–water nanofluid as the working fluid and Triton X-100 as surfactant by nanoparticle volume fractions of 0.2 and 0.4% and particle dimension of 15 nm on the efficiency of a flat-plate solar collector. They showed that at nanoparticles concentration of 0.2% the solar collector efficiency increased to 28.3%.

Mathematical modeling

Geometry description

Commonly evacuated solar collector modules are used as categories of evacuated tube collectors. A schematic diagram of the present study's evacuated solar collector module is shown in Fig. 1, where the number of evacuated solar tubes is between 15 and 40 at each module.

Governing equations

- Continuity equation

$$\frac{\partial \rho}{\partial t} + \nabla.(\rho \vec{v}) = 0 \tag{1}$$

- Momentum equation

$$\frac{\partial}{\partial t}(\rho \vec{v}) + \nabla.(\rho \vec{v}) = -\nabla p + \nabla.(\bar{\tau}) + p\vec{g} + \vec{F} \tag{2}$$

- Energy equation

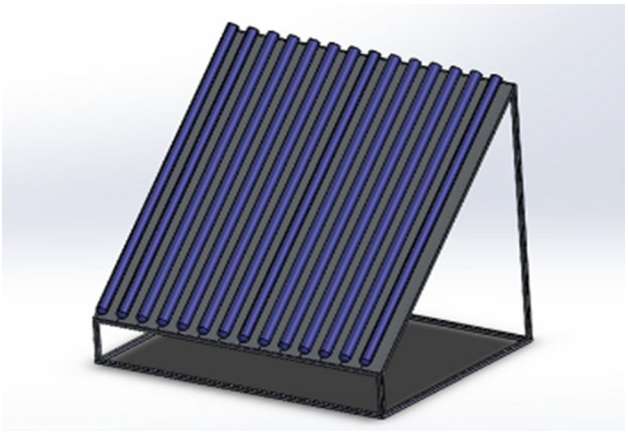

Fig. 1 A schematic diagram of the evacuated solar collector module in this study

$$\frac{\partial}{\partial t}(\rho E) + \nabla.(\vec{v}(\rho E + P)) = \nabla.(k\nabla T + (\bar{\tau}.\bar{v})) + S_h \tag{3}$$

- Radiation equation

The radiation equation for emitter, absorber and transmittal environments at place of $\vec{r}$ and direction of $\vec{s}$ is defined as below.

$$\frac{\mathrm{d}I(\vec{r},\vec{s})}{\mathrm{d}s} + (a+\sigma_s)I(\vec{r},\vec{s}) = an^2\frac{\sigma T^4}{\pi} + \frac{\sigma_s}{4\pi}\int_0^{4\pi} I(\vec{r},\vec{s}')\mathrm{d}\Omega' \tag{4}$$

where parameters of n, a, σ and σ_s are refractive coefficient, absorption coefficient, Stefan–Boltzmann constant and transmission coefficient, respectively.

Boundary conditions

The velocity inlet with a uniform velocity or mass flow rate and temperature is fixed as the inlet boundary condition, while pressure outlet with zero gauge pressure is considered as the outlet boundary condition; besides, the flow is fully developed.

The input energy into the collector consists of two parts. Part of the energy is formed by the direct radiation energy, and the other part is provided by a reflector mounted underneath the light. The solar radiation is considered to radiate directly. The numerical data of Windows and the experimental data are used to distribute the radiation angle around the collector. The following equations show the angular distribution as the boundary condition of the outer surface of solar collector:

$$q''(\theta) = \begin{cases} q_m(0.41\cos(2\theta) + 0.59); & 0 \le \theta \le \frac{\pi}{2} \\ q_m(0.16\cos(2\theta) + 0.34); & \frac{\pi}{2} \le \theta \le \pi \end{cases} \tag{5}$$

Thermo-physical properties

The thermo-physical properties of the present nanofluid which flows into the solar collector are considered as a function of temperature. Equations (6), (7), (8) and (9) show the nanofluid thermo-physical properties including density, specific heat capacity, effective dynamic viscosity and effective thermal conductivity from Maxwell correlation, respectively.

$$\rho_{nf} = (1-\phi)\rho_f + \varphi\rho_s \tag{6}$$

$$(\rho C_p) = (1-\phi)(\rho C_p)_f + \phi(\rho C_p)_s \tag{7}$$

$$\mu_{nf} = \frac{\mu_f}{(1-\phi)^{2.5}} \tag{8}$$

$$\frac{k_{nf}}{k_f} = \frac{k_p + 2k_f - 2\phi(k_f - k_p)}{k_p + 2k_f + \phi(k_f - k_p)} \tag{9}$$

The thermo-physical properties of the water are considered as a function of temperature ranging from 0 to 150 °C. Equations (10), (11), (12) and (13) present the water density, specific heat capacity, effective dynamic viscosity and effective thermal conductivity, respectively.

$$\rho_f = a + bT + cT^2 + dT^{2.5} + eT^3 \tag{10}$$

$$C_{p,f} = a + bT + cT^2 + dT^3 + eT^4 \tag{11}$$

$$\mu_f = (a + bT + cT^2 + dT^3)^{-1} \tag{12}$$

$$k_f = a + bT + cT^{1.5} + dT^2 + eT^{0.5} \tag{13}$$

Numerical procedure

In this study, the computational fluid dynamic is utilized for the three-dimensional simulation. To discretize the partial deferential equations, the finite volume method with the commercial software of Ansys Fluent version 17.0 is employed. The nanofluid simulation has been performed under single-phase model, and the fluid flow is assumed to be steady and incompressible under laminar regime [15–61]. The grid study and validation sections are presented as follows.

Grid study

The grid independency is investigated by analyzing the effect of the grid size on numerical results. Due to the high temperature and velocity gradients near the walls of the solar collector, smaller mesh is implemented in these regions. Moreover, the hexagonal and edge shape for 3D meshing is used. The outlet temperate of the collector is analyzed through different element numbers including

634,286–1,347,288–1,910,724. The results showed that the differences between the second and third cases in solar collector outlet temperature are subtle, so this number of elements suffices for the subsequent computations due to its relative error. The generated mesh in solar collector cross section is displayed in Fig. 2.

Validation

To validate the present numerical study, it has been compared to the experimental study of Liang et al. [12]. Figure 3 presents the cross-sectional and longitudinal section views of their U-shaped evacuated tube solar collector composed of three solid regions and two fluid regions. Fluid region consists of the air between the two tubes and the working fluid flows into the U-shaped tube, and the solid region consists of one region filled by compressed graphite and two glass tubes.

The experimental data of the U-shaped evacuated tube solar collector efficiency versus inlet and outlet temperature difference are compared to the present numerical results in Fig. 4a. Environment temperature, radiation intensity and fluid are considered to be constant. Due to reach the different values of decreased temperature, the fluid inlet temperature is considered to be variable. Furthermore, Fig. 4b displays the comparison between the present numerical data and the experimental results for the solar collector inlet and outlet temperature difference versus fluid mass flow rate at radiation intensity and fluid inlet temperature of 900 W m^{-2} and 308 K, respectively. The good agreement between the present numerical results and experimental data proves the validity of the present numerical simulation considering the variability of outdoor working conditions and the mentioned simplifications.

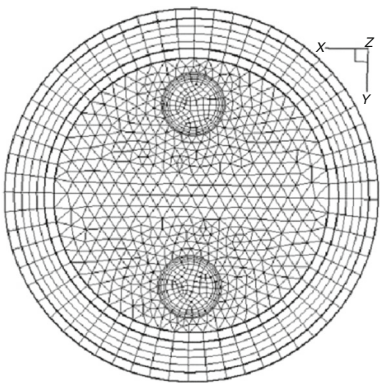

Fig. 2 The present study generated mesh in the solar collector

Results and discussion

At this stage, the effects of the geometrical properties of the solar collector including diameter and length of the U-shaped tubes and also the effects of nanoparticles of CuO, TiO_2 and Al_2O_3 with various volume concentrations dispersed in water on the solar collector thermal performance will be evaluated.

Figure 5 presents the fluid velocity in the route forth and back in the U-shaped tubes of the solar collector. At the inlet section, fluid enters uniformly, and hence, it needs to get fully developed hydrodynamically by surpassing the entrance region; besides, it is also visible at the first step of each cycle of the fluid route forth and back. In addition, in this figure a line as presenting the hydrodynamic fully developed flow through the entire fluid route is shown to be compared to the real velocity distribution. It is also noteworthy that the sudden change in the direction of the velocity curve is because of reaching the fluid to the end of the U-shaped tube.

Figure 6 displays the effect of the solar collector length on its efficiency versus the inlet and outlet temperature differences. Three lengths including 1000, 1450, 2000 mm for the solar collector are considered under environment temperature, radiation intensity and mass flow rate of 303 K, 500 W m^{-2} and 0.005 kg s^{-1}, respectively. Based on this figure, increasing the collector length enhances its efficiency. In fact, augmenting the collector length decreases the effects of the first and last regions of the collector. Moreover, this figure illustrates that increasing the collector length from 1000–1450 and 1450–2000 mm causes 7.3 and 8.4% enhancement in its efficiency,

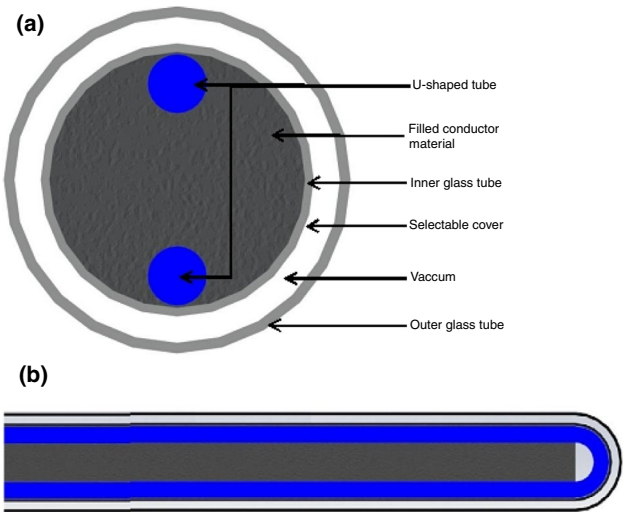

Fig. 3 The **a** cross-sectional and **b** longitudinal section views of the U-shaped evacuated tube solar collector of Liang et al. [12] study

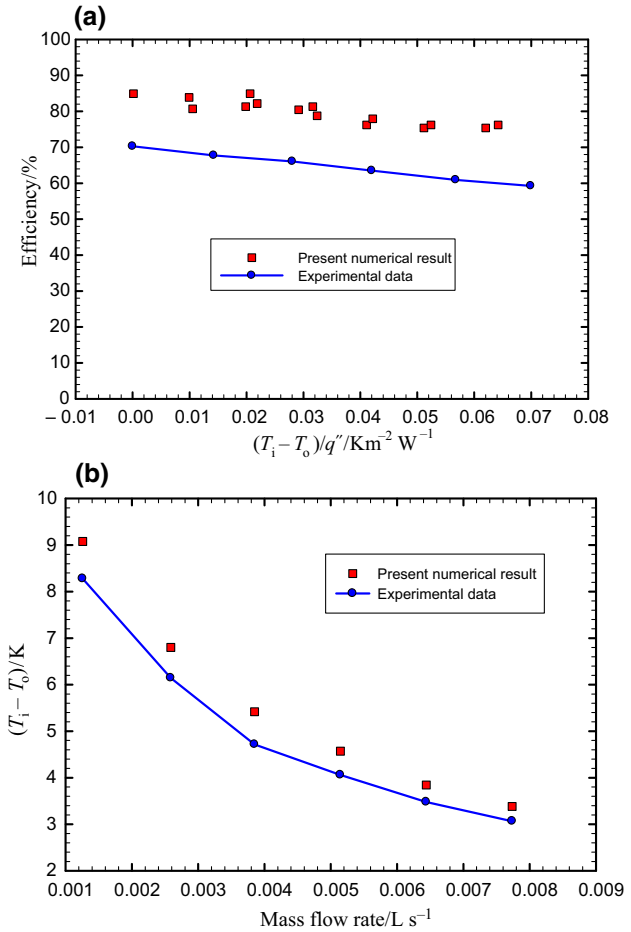

Fig. 4 Comparisons of the present numerical simulation to the experimental data of Liang et al. [13]

respectively, for the highest inlet and outlet temperature difference.

Figure 7 shows the effect of solar collector diameter on its efficiency versus the inlet and outlet temperature differences. Three collector diameters of 23.5, 47 and 94 mm are investigated under environment temperature, radiation intensity and mass flow rate of 303 K, 500 W m^{-2} and 0.005 kg s^{-1}, respectively. This figure demonstrates that the more the collector diameter, the more its efficiency. In addition, enhancing the collector diameter from 23.5–47 and 47–94 mm causes 7.5 and 5.3% enhancement in its efficiency, respectively, for the highest inlet and outlet temperature difference.

In order to investigate the effects of oxide nanofluids on the solar collector thermal performance, nanoparticles of CuO, TiO_2 and Al_2O_3 dispersed in water are considered with volume fractions of 0.1–4%.

The effect of CuO–water nanofluid with different nanoparticles volume fractions on the solar collector efficiency is shown in Fig. 8. It shows that using this type of nanofluid causes an enhancement in the collector efficiency

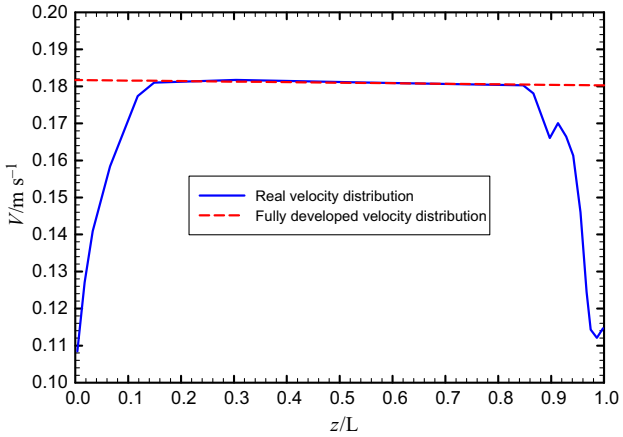

Fig. 5 Velocity distribution of fluid flow through the entire U-shaped tube of the solar collector

in which it increases up to 13.3% in the nanoparticles volume fraction of 4% in comparison with using water as the working fluid.

Figure 9 shows the effect of TiO_2–water nanofluid with different nanoparticles volume fractions on the solar collector efficiency. This type of nanofluid leads to an increase in the collector efficiency as well in which it increases up to 9.1% in the nanoparticles volume fraction of 4% in comparison with using water as the working fluid.

The effect of the third type of nanofluid named Al_2O_3–water with different nanoparticles volume fractions on the solar collector efficiency is presented in Fig. 10. Like the other two types of nanofluids, using this one also increases the efficiency of the solar collector, while this type of nanofluid enhances the collector efficiency up to 10.7% in 4% nanoparticles volume fraction in comparison with using water as the working fluid.

To compare the three nanofluids performance and effect on thermal efficiency of the solar collector, Fig. 11 is

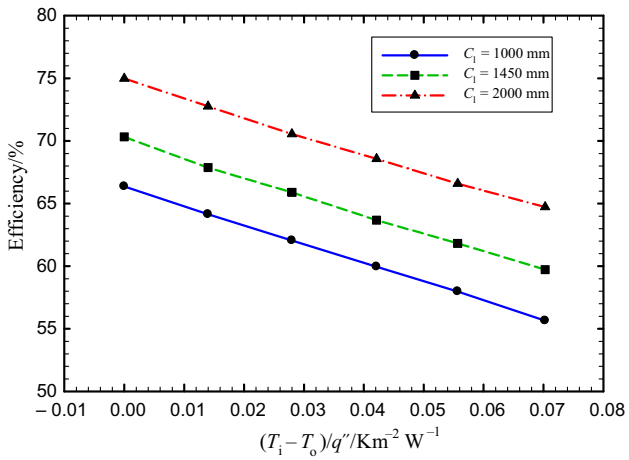

Fig. 6 Variations of the solar collector efficiency with the collector temperature differences for different collector lengths

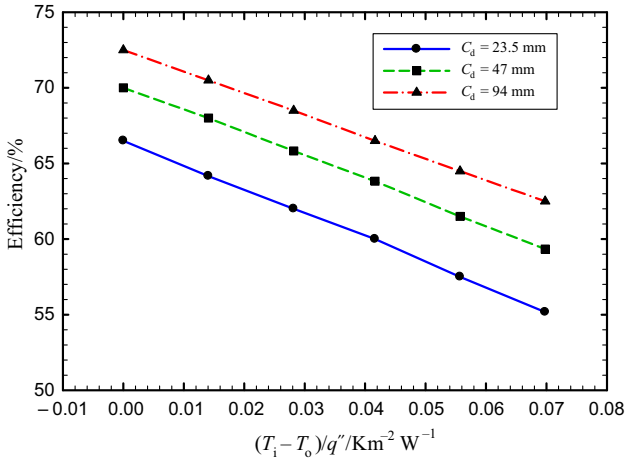

Fig. 7 Variations of the solar collector efficiency with the collector temperature differences for different collector diameters

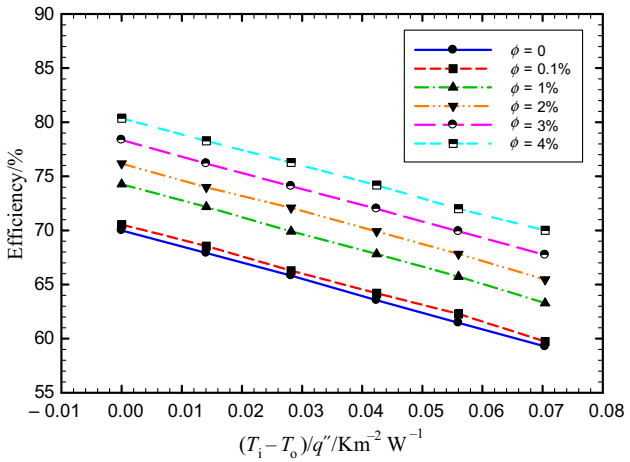

Fig. 8 Variations of the solar collector efficiency with the collector temperature differences for CuO–water nanofluid in different nanoparticle volume fractions

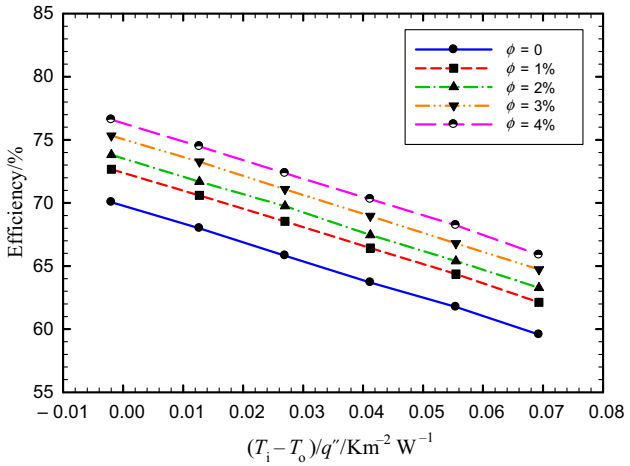

Fig. 9 Variations of the solar collector efficiency with the collector temperature differences for Al_2O_3–water nanofluid in different nanoparticle volume fractions

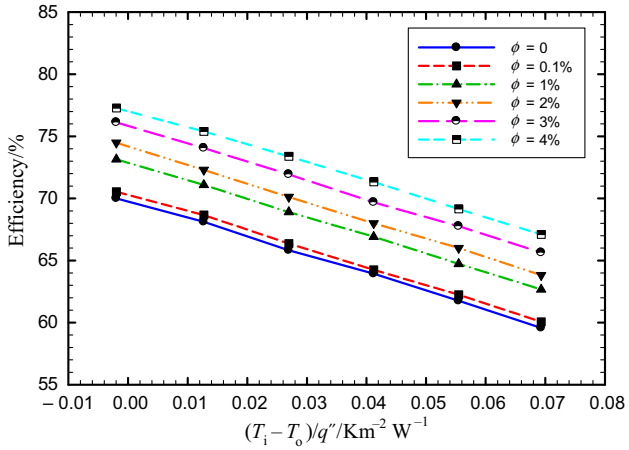

Fig. 10 Variations of the solar collector efficiency with the collector temperature differences for TiO_2–water nanofluid in different nanoparticle volume fractions

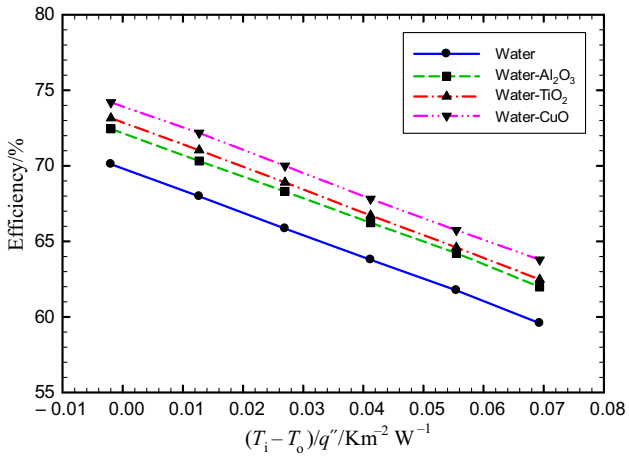

Fig. 11 Variations of the solar collector efficiency with the collector temperature differences for pure water and three oxide nanofluids with nanoparticle volume fractions of 1%

shown in nanoparticles volume fraction of 1%. This figure displays that the nanofluid of CuO–water leads to the highest collector efficiency and its efficiency is 1.3 and 1.5% higher than TiO_2–water and Al_2O_3–water nanofluids, respectively. It is noteworthy that the CuO–water nanofluid has the least heat capacity than the other two types of nanofluids and it shows that the working fluid heat capacity has an important effect on the evacuated tube solar collector.

Conclusions

This is a three-dimensional numerical study of a U-shaped tube solar collector using three different types of nanofluids including CuO–water, Al_2O_3–water and TiO_2–water with

volume concentrations ranging from 0.1 to 4%. The environment temperature, radiation intensity and mass flow rate are fixed to 303 K, 500 W m^{-2} and 0.005 kg s^{-1}, respectively. The thermal efficiency of the solar collector was evaluated under different solar collector lengths (1000, 1450, 2000 mm) and diameters (23.5, 47, 94 mm). The obtained results are summarized below:

1. Increasing both length and diameter of the U-shaped tube solar collector enhances its thermal performance.
2. Using nanofluids as the working fluid flowing in the U-shaped tube solar collector and also increasing the nanoparticles volume fraction result in an augmentation in the collector thermal efficiency.
3. Among the three evaluated nanofluid, CuO–water nanofluid reaches the highest thermal performance of the solar collector, then it follows by TiO_2–water nanofluid, and finally, Al_2O_3–water accounts for the least solar collector thermal efficiency.

Acknowledgements The first author acknowledges the support provided by the NSFC (51905351), Natural Science Foundation of Guangdong Province, China (2018A030310522), Shenzhen Science and Technology Planning Project, China (JCYJ20170818100522101) and Natural Science Foundation of Shenzhen University (2017032).

References

1. Morrison G, Budihardjo I, Behnia M. Water-in-glass evacuated tube solar water heaters. Sol Energy. 2004;76(1):135–40.
2. Morrison G, Budihardjo I, Behnia M. Measurement and simulation of flow rate in a water-in-glass evacuated tube solar water heater. Sol Energy. 2005;78(2):257–67.
3. Budihardjo I, Morrison GL, Behnia M. Natural circulation flow through water-in-glass evacuated tube solar collectors. Sol Energy. 2007;81(12):1460–72.
4. Benedetto D, Shah D, Kaufman H. The instilled fluid dynamics and surface chemistry of polymers in the preocular tear film. Invest Ophthalmol Vis Sci. 1975;14(12):887–902.
5. Ong K, Chow C. Performance of a solar chimney. Sol Energy. 2003;74(1):1–17.
6. Sabat FM. Evacuated heatpipe solar collector. Google Patents. 1982.
7. Rittidech S, et al. Correlation to predict heat transfer characteristics of a closed-end oscillating heat pipe at normal operating condition. Appl Therm Eng. 2003;23(4):497–510.
8. Hayek M, Assaf J, Lteif W. Experimental investigation of the performance of evacuated-tube solar collectors under eastern mediterranean climatic conditions. Energy Procedia. 2011;6:618–26.
9. Sawhney R, Bansal N. Performance parameters of an evacuated tubular collector with a U-tube fluid channel. J Sol Energy Eng. 1987;109(4):346–8.
10. Qu J, Wu H. Thermal performance comparison of oscillating heat pipes with SiO_2/water and Al_2O_3/water nanofluids. Int J Therm Sci. 2011;50(10):1954–62.
11. Diaz G. Performance analysis and design optimization of a minichannel evacuated-tube solar collector. In: Proceedings of ASME IMECE. 2008.
12. Liang R, et al. Theoretical and experimental investigation of the filled-type evacuated tube solar collector with U tube. Sol Energy. 2011;85(9):1735–44.
13. Liang R, et al. Performance analysis of a new-design filled-type solar collector with double U-tubes. Energy Build. 2013;57:220–6.
14. Yousefi T, et al. An experimental investigation on the effect of Al_2O_3–H_2O nanofluid on the efficiency of flat-plate solar collectors. Renew Energy. 2012;39(1):293–8.
15. Shadloo MS. Numerical simulation of compressible flows by lattice Boltzmann method. Numer Heat Transf A. 2019;75(3):167–82.
16. Hopp-Hirschler M, Shadloo MS, Nieken U. Viscous fingering phenomena in the early stage of polymer membrane formation. J Fluid Mech. 2019;864:97–140.
17. Sadeghi R, Shadloo MS, Hopp-Hirschler M, Hadjadj A, Nieken U. Three-dimensional lattice Boltzmann simulations of high density ratio two-phase flows in porous media. Comput Math Appl. 2018;75:2445–65.
18. Hopp-Hirschler M, Shadloo MS, Nieken U. A smoothed particle hydrodynamics approach for thermo-capillary flows. Comput Fluids. 2018;176:1–19.
19. Toghyani S, Afshari E, Baniasadi E, Shadloo MS. Energy and exergy analyses of a nanofluid based solar cooling and hydrogen production combined system. Renew Energy. 2019;141:1013–25.
20. Nasiri H, Jamalabadi MYA, Sadeghi R, Safaei MR, Shadloo MS. A smoothed particle hydrodynamics approach for numerical simulation of nano-fluid flows: application to forced convection heat transfer over a horizontal cylinder. J Therm Anal Calorim. 2018. https://doi.org/10.1007/s10973-018-7022-4.
21. Piquet A, Zebiri B, Hadjadj A, Shadloo MS. A parallel high-order compressible flows solver with a domain decomposition method in the generalized curvilinear coordinates system. Int J Numer Methods Heat Fluid Flow. 2019. https://doi.org/10.1108/hff-01-2019-0048.
22. Shenoy DV, Shadloo MS, Hadjadj A, Peixinho J. Direct numerical simulations of laminar and transitional flows in diverging pipes. Int J Numer Methods Heat Fluid Flow. 2019. https://doi.org/10.1108/hff-02-2019-0111.
23. Nguyen MQ, Shadloo MS, Hadjadj A, Lebon B, Peixinho J. Perturbation threshold and hysteresis associated with the transition to turbulence in sudden expansion pipe flow. Int J Heat Fluid Flow. 2019;76:187–96.
24. Lebon B, Nguyen MQ, Peixinho J, Shadloo MS, Hadjadj A. A new mechanism for the periodic bursting of the recirculation region of the flow through a sudden expansion in a circular pipe. Phys Fluids. 2018;30:031701.
25. Sharma S, Shadloo MS, Hadjadj A, Kloker MJ. Control of oblique-type breakdown in a supersonic boundary layer employing streaks. J Fluid Mech. 2019;1:1. https://doi.org/10.1017/jfm.2019.435.
26. Mendez-Gonzlez M, Shadloo MS, Hadjadj A, Ducoin A. Boundary layer transition over a concave plate caused by centrifugal instabilities. Comput Fluids. 2018;171:135–53.
27. Shadloo MS, Hadjadj A. Laminar-Turbulent transition in supersonic boundary layers with surface heat transfer: a numerical study. Numer Heat Transf A Appl. 2017;72(1):40–53.
28. Rashidi MM, Nasiri M, Shadloo MS, Yang Z. Entropy generation in a circular tube heat exchanger using nanofluids: effects of different modeling approaches. Heat Transf Eng. 2017;38(9):853–66.
29. Shadloo MS, Oger G, Le Touze D. Smoothed particle hydrodynamics method for fluid flows, towards industrial applications: motivations, current state, and challenges. Comput Fluids. 2016;136:11–34.

30. Karimipour A, Bagherzadeh SA, Taghipour A, Abdollahi A, Safaei MR. A novel nonlinear regression model of SVR as a substitute for ANN to predict conductivity of MWCNT-CuO/water hybrid nanofluid based on empirical data. Physica A. 2019;521:89–97.
31. Safaei MR, Karimipour A, Abdollahi A, Nguyen TK. The investigation of thermal radiation and free convection heat transfer mechanisms of nanofluid inside a shallow cavity by lattice Boltzmann method. Physica A. 2018;509:515–35.
32. Jiang Y, Bahrami M, Bagherzadeh SA, Abdollahi A, Sulgani MT, Karimipour A, Goodarzi M, Bach QV. Propose a new approach of fuzzy lookup table method to predict Al_2O_3/deionized water nanofluid thermal conductivity based on achieved empirical data. Physica A. 2019;527:121177.
33. Salimpour MR, Karimi Darvanjooghi MH, Abdollahi A, Karimipour A, Goodarzi M. Providing a model for C_{sf} according to pool boiling convection heat transfer of water/ferrous oxide nanofluid using sensitivity analysis. Int J Numer Methods Heat Fluid Flow. 2019. https://doi.org/10.1108/HFF-01-2019-0009.
34. Mozaffari M, D'Orazio A, Karimipour A, Abdollahi A, Safaei MR. Lattice Boltzmann method to simulate convection heat transfer in a microchannel under heat flux: gravity and inclination angle on slip-velocity. Int J Numer Methods Heat Fluid Flow. 2019. https://doi.org/10.1108/HFF-12-2018-0821.
35. Tian Z, Bagherzadeh SA, Ghani K, Karimipour A, Abdollahi A, Bahrami M, Safaei MR. Nonlinear function estimation fuzzy system (NFEFS) as a novel statistical approach to estimate nanofluids' thermal conductivity according to empirical data. Int J Numer Methods Heat Fluid Flow. 2019. https://doi.org/10.1108/HFF-12-2018-0768.
36. Aghakhani S, Pordanjani AH, Karimipour A, Abdollahi A, Afrand M. Numerical investigation of heat transfer in a power-law non-Newtonian fluid in a C-Shaped cavity with magnetic field effect using finite difference lattice Boltzmann method. Comput Fluids. 2018;176:51–67.
37. Dehkordi BAF, Abdollahi A. Experimental investigation toward obtaining the effect of interfacial solid-liquid interaction and basefluid type on the thermal conductivity of CuO-loaded nanofluids. Int Commun Heat Mass Transf. 2018;97:151–62.
38. Abdollahi A, Darvanjooghi MHK, Karimipour A, Safaei MR. Experimental study to obtain the viscosity of CuO-loaded nanofluid: effects of nanoparticles' mass fraction, temperature and basefluid's types to develop a correlation. Meccanica. 2018;53(15):3739–57.
39. Dehghani Y, Abdollahi A, Karimipour A. Experimental investigation toward obtaining a new correlation for viscosity of WO_3 and Al_2O_3 nanoparticles-loaded nanofluid within aqueous and non-aqueous basefluids. J Therm Anal Calorim. 2019;135(1):713–28.
40. Sedeh RN, Abdollahi A, Karimipour A. Experimental investigation toward obtaining nanoparticles' surficial interaction with basefluid components based on measuring thermal conductivity of nanofluids. Int Commun Heat Mass Transf. 2019;103:72–82.
41. Norouzipour A, Abdollahi A, Afrand M. Experimental study of the optimum size of silica nanoparticles on the pool boiling heat transfer coefficient of silicon oxide/deionized water nanofluid. Powder Technol. 2019;345:728–38.
42. Bahrami M, Akbari M, Bagherzadeh SA, Karimipour A, Afrand M, Goodarzi M. Develop 24 dissimilar ANNs by suitable architectures & training algorithms via sensitivity analysis to better statistical presentation: measure MSEs between targets & ANN for Fe–CuO/Eg–water nanofluid. Physica A. 2019;519:159–68.
43. Jalali E, Karimipour A. Simulation the effects of cross-flow injection on the slip velocity and temperature domain of a nanofluid flow inside a microchannel. Int J Numer Methods Heat Fluid Flow. 2019;29(5):1546–62.
44. Pordanjani AH, Aghakhani S, Karimipour A, Afrand M, Goodarzi M. Investigation of free convection heat transfer and entropy generation of nanofluid flow inside a cavity affected by magnetic field and thermal radiation. J Therm Anal Calorim. 2019;137(3):997–1019.
45. Safaei MR, Ranjbarzadeh R, Hajizadeh A, Bahiraei M, Afrand M, Karimipour A. Effects of cobalt ferrite coated with silica nanocomposite on the thermal conductivity of an antifreeze: new nanofluid for refrigeration condensers. Int J Refrig. 2019;102:86–95.
46. Bagherzadeh SA, D'Orazio A, Karimipour A, Goodarzi M, Bach QV. A novel sensitivity analysis model of EANN for F-MWCNTs–Fe_3O_4/EG nanofluid thermal conductivity: outputs predicted analytically instead of numerically to more accuracy and less costs. Physica A. 2019;521:406–15.
47. Gholamalizadeh E, Pahlevanzadeh F, Ghani K, Karimipour A, Nguyen TK, Safaei MR. Simulation of water/FMWCNT nanofluid forced convection in a microchannel filled with porous material under slip velocity and temperature jump boundary conditions. Int J Numer Methods Heat Fluid Flow. 2019. https://doi.org/10.1108/HFF-01-2019-0030
48. Goodarzi M, Javid S, Sajadifar A, Nojoomizadeh M, Motaharipour SH, Bach QV, Karimipour A. Slip velocity and temperature jump of a non-Newtonian nanofluid, aqueous solution of carboxy-methyl cellulose/aluminum oxide nanoparticles, through a microtube. Int J Numer Methods Heat Fluid Flow. 2019;29(5):1606–28.
49. Alrashed AA, Karimipour A, Bagherzadeh SA, Safaei MR, Afrand M. Electro-and thermophysical properties of water-based nanofluids containing copper ferrite nanoparticles coated with silica: experimental data, modeling through enhanced ANN and curve fitting. Int J Heat Mass Transf. 2018;127:925–35.
50. Karimipour A, Bagherzadeh SA, Goodarzi M, Alnaqi AA, Bahiraei M, Safaei MR, Shadloo MS. Synthesized CuFe2O4/SiO2 nanocomposites added to water/EG: evaluation of the thermophysical properties beside sensitivity analysis & EANN. Int J Heat Mass Transf. 2018;127:1169–79.
51. Hamlehdar M, Kasaeian A, Safaei MR. Energy harvesting from fluid flow using piezoelectrics: a critical review. Renew Energy. 2019;143:1826–38.
52. Goodarzi H, Akbari OA, Sarafraz MM, Karchegani MM, Safaei MR, Shabani GAS. Numerical simulation of natural convection heat transfer of nanofluid with Cu, MWCNT, and Al_2O_3 nanoparticles in a cavity with different aspect ratios. J Therm Sci Eng Appl. 2019;11(6):061020.
53. Sarafraz MM, Safaei MR. Diurnal thermal evaluation of an evacuated tube solar collector (ETSC) charged with graphene nanoplatelets-methanol nano-suspension. Renew Energy. 2019;142:364–72.
54. Mozaffari M, Karimipour A, D'Orazio A. Increase lattice Boltzmann method ability to simulate slip flow regimes with dispersed CNTs nanoadditives inside. J Therm Anal Calorim. 2019;137(1):229–43.
55. Arabpour A, Karimipour A, Toghraie D, Akbari OA. Investigation into the effects of slip boundary condition on nanofluid flow in a double-layer microchannel. J Therm Anal Calorim. 2018;131(3):2975–91.
56. Hassani M, Karimipour A. Discrete ordinates simulation of radiative participating nanofluid natural convection in an enclosure. J Therm Anal Calorim. 2018;134(3):2183–95.
57. Arasteh H, Mashayekhi R, Toghraie D, Karimipour A, Bahiraei M, Rahbari A. Optimal arrangements of a heat sink partially filled with multilayered porous media employing hybrid nanofluid. J Therm Anal Calorim. 2019;137(3):1045–58.
58. Goodarzi M, Toghraie D, Reiszadeh M, Afrand M. Experimental evaluation of dynamic viscosity of ZnO–MWCNTs/engine oil

hybrid nanolubricant based on changes in temperature and concentration. J Therm Anal Calorim. 2019;136(2):513–25.
59. Nasiri H, Jamalabadi MYA, Sadeghi R, Safaei MR, Nguyen TK, Shadloo MS. A smoothed particle hydrodynamics approach for numerical simulation of nano-fluid flows. J Therm Anal Calorim. 2019;135(3):1733–41.
60. Sharma S, Shadloo MS, Hadjadj A. Turbulent flow topology in supersonic boundary layer with wall heat transfer. Int J Heat Fluid Flow. 2019;78:108430.
61. Sarafraz MM, Tian Z, Tlili I, Kazi S, Goodarzi M. Thermal evaluation of a heat pipe working with *n*-pentane-acetone and *n*-pentane-methanol binary mixtures. J Therm Anal Calorim. 2019. https://doi.org/10.1007/s10973-019-08414-2.